Enhanced Beam Widening Approach for RIS-Assisted Wireless Communication Systems

Hanlin Guan, Maarouf Al Hajj, Valéry Guillet, Hmaied Shaiek

4th URSI AT-RASC, Gran Canaria, 19 – 24 May 2024

Enhanced Beam Widening Approach for RIS-Assisted Wireless Communication Systems

Hanlin Guan*(1), Maarouf Al Hajj(2)[1], Valéry Guillet(2), and Hmaied Shaiek(1)
(1) Conservatoire National des Arts et Métiers (CNAM), Paris, France
(2) Orange Labs, Belfort, France

Abstract

In recent years, there have been numerous theoretical innovations and prototype testing efforts that have demonstrated the advantages of Reconfigurable Intelligent Surfaces (RIS) technology in terms of low cost, low power, and ease of deployment, as well as numerous potential opportunities and broad application prospects for future 6G networks. However, implementing beamforming with RIS can be challenging, especially in the case of beam widening requirements. This paper proposes a dedicated Genetic Algorithms (GA)-based algorithm for beamwidening in RIS-based communications. The main idea of this paper, with respect to previous studies published in the literature is that it ensures an enhanced control of wide beam characteristics by adjusting the constraints of the cost function optimized by GA.

Keywords— Reconfigurable Intelligent Surface (RIS), Beamforming, Beam Widening, Genetic Algorithms (GA), Wireless Communications

1 Introduction

6G and future generations of telecommunications are expected to operate at higher frequencies, potentially ranging from 10 GHz to 30 THz. However, higher frequencies can result in shorter signal transmission distances and lower communication link quality due to high path loss and limited coverage. Currently, there are several solutions available to address the issue of path loss in high-frequency bands, including Ultra-Scale Multiple-Input Multiple-Output (MIMO) and Reconfigurable Intelligent Surfaces (RIS) [1].

RIS is an artificial electromagnetic hypersurface that can flexibly regulate the amplitude, phase, polarization, and frequency of spatial electromagnetic waves. It has gained significant attention in academia and industry due to its advantages of low cost, low power consumption, tunability, and high reliability. RIS can be deployed in the wireless signal transmission path to improve the scattering conditions of the channel passively, enhancing the multiplexing gain of the communication system. Additionally, it can actively regulate the signals on the propagation path, effectively eliminating signal blind zones, enhancing received signals, and improving the performance of communication transmission through channel regulation.

[1]Contribution made when the author was affiliated with Orange Labs, current affiliation is with Ericsson France.

The transmitter and reflector arrays are a subset of the RIS technology. Transmit and reflect arrays have lower cost and power consumption compared to the all-digital massive MIMO solution. They act as antennas with many reconfigurable elements, focusing the radiated energy in a specific direction in space. This produces a very narrow, highly directional beam that can counteract propagation path losses. However, narrow beams are more susceptible to obstruction and may have increased overhead due to longer scan times. They are also more susceptible to pointing errors due to user mobility.

To overcome these limitations, researchers are investigating beam widening techniques. The goal is to obtain wide beams that can be used for applications such as cell or sector-wide broadcasting. Commonly used methods for optimization include the phase-array method [2], amplitude-array method [3], phase-amplitude array method [3], element grouping method [4], and so on. Some studies have also utilized genetic algorithms (GA) [5] and neural networks [6].

The method proposed in this paper builds upon the work done in [5], which proposes GA-based optimization to generate codebooks with wide beams by phase-only tapering of 1-bit coded transmitter array antennas while ensuring minimum levels of sidelobes and beam ripples. The idea of this paper is to adjust the parameters of the loss function and the GA in order to get better beam characteristics, especially out-off the RIS broadside. The structure of this paper is the following. In section II, we introduce the system model and basic concepts, in section III we explain the optimization problem formulation, section IV presents simulation results, before concluding in section V.

2 System Model

2.1 Transmit array RIS system model

This paper considers a general RIS-assisted single-input single-output (SISO) wireless communication system in a transmitting array (TA) scenario, as shown in Figure 1. This paper considers a square RIS operating in the 26 GHz band with dimensions $M = N = 20$, where M and N denote the number of rows and columns of regularly arranged cells in the RIS, respectively. The RIS is positioned in the x-y plane of the Cartesian coordinate system, with the geometric center of the RIS located at the origin of the coordinate system. Each cell has a dimension d_x along the x-axis and d_y along the y-axis. In this paper, we use $d_x = d_y = \lambda/2$. We denote by $D = \max(M \times d_x, N \times d_y)$ the maximum width of the RIS. A transmit horn antenna is located on the negative z-axis at a focal distance of F, which is a function of D and the radiation pattern of the horn antenna used [7]. The optimal value of F/D

for a square array of 20×20 UC when using one horn antenna is 0.47 [7].

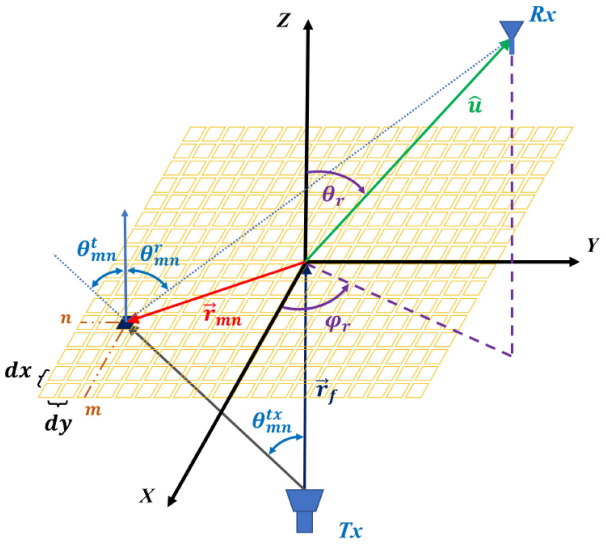

Figure 1. An illustration of the transmitarray's system model [5].

2.2 Electric field

In this paper, we only consider the far-field transmission case, which means that the distance from the receiver to the center of the RIS will be greater than the boundary between the far and near fields, determined by $L = 2D^2/\lambda$.

Since the original equation for calculating the electric field involves double summation [8], we use 2D Fast Fourier Inverse Transform (2D-IFFT) instead of double summation to simplify and speed up the calculation, which also transforms the directions (θ_r, φ_r) into the corresponding angular coordinates (u, v), thus resulting in [9]

$$E(u,v) = (1-u^2-v^2)^{1/2} M.N \times \text{IFFT}\Big[\frac{F^{tx}(\theta^{tx}_{mn})F^t(\theta^t_{mn})}{\|\vec{r}_{mn}-\vec{r}_f\|} \times e^{j\Phi_{mn}-jk\|\vec{r}_{mn}-\vec{r}_f\|}\Big], \tag{1}$$

where

$$u = \sin(\theta_r)\cos(\phi_r) = \frac{2\pi}{N^{FFT}_x d_x k} p, \quad v = \sin(\theta_r)\sin(\phi_r) = \frac{2\pi}{N^{FFT}_y d_y k} q, \tag{2}$$

$$p = -\frac{N^{FFT}_x - 1}{2}, -\frac{N^{FFT}_x - 1}{2} + 1, \ldots \frac{N^{FFT}_x - 1}{2}, \quad q = -\frac{N^{FFT}_y - 1}{2}, -\frac{N^{FFT}_y - 1}{2} + 1, \ldots \frac{N^{FFT}_y - 1}{2}, \tag{3}$$

$$F^{tx}(\theta^{tx}_{mn}) = \cos^4(\theta^{tx}_{mn}), \tag{4}$$

and

$$F^x(\theta^x_{mn}) = \frac{4\pi A_{phy}}{\lambda^2}\cos(\theta^x_{mn}). \tag{5}$$

$F^{tx}(\theta^{tx}_{mn})$ is the radiation pattern of Tx where θ^{tx}_{mn} is the elevation angle from the Tx to the $(m,n)^{th}$ UC, $F^x(\theta^x_{mn})$ are the radiation patterns of UCs where $x \in \{t, r\}$ is for transmission or reception respectively and θ^x_{mn} is the elevation angle from the $(m,n)^{th}$ UC to the Tx or Rx, A_{phy} is the physical area of the UC, N^{FFT}_x and N^{FFT}_y are the output shapes of the FFT in the x and y directions, respectively.

3 Optimization problems

This section presents a Genetic Algorithm (GA) approach defined in [5] to optimize the phase matrix of the UCs to obtain a radiation pattern with a lower Side Lobe Level (SLL) and specific constraints on the Half-Power Beamwidth (HPBW). The objective of this section is to improve the performances shown in [5], by adjusting the parameters of the GA algorithm and the cost function.

This paper utilizes the GA to compute the phase matrix of UCs. GA is a stochastic adaptive global search optimization method that models the process of biological evolution in nature. It was originally developed from computer simulation studies on biological systems, which simulate the phenomena of replication, crossover, and mutation that occur in natural selection and inheritance [11].

The computation of the phase matrix can be transformed into an optimization problem. The stochasticity in the algorithm helps to find the global minimum, providing the matrix with the best performance for the RIS. The objective function is to minimize the difference between the computed radiation pattern and a predetermined desired radiation pattern. Since we are mainly concerned with SLL and HPBW, the objective function of GA can be written as

$$F_{obj} = \sum_{(u,v)\in S_L}\left(\frac{\hat{E}(u,v) - M_L(u,v)}{|S_L|}\right)^2 + \sum_{(u,v)\in S_U}\left(\frac{\hat{E}(u,v) - M_U(u,v)}{|S_U|}\right)^2, \tag{6}$$

where

$$S_L = \{(u,v) \mid \hat{E}(u,v) < M_L(u,v)\}, \quad S_U = \{(u,v) \mid \hat{E}(u,v) > M_U(u,v)\}, \tag{7}$$

and $\hat{E}$ is the normalized radiation pattern, with M_L and M_U are the lower and upper masks containing the given metrics HPBW and SLL, respectively. S_L is the region which applies only to where $\hat{E}$ is less than M_L, while S_U is the region which applies only to where $\hat{E}$ is greater than M_U. The operator $|\cdot|$ denotes the cardinality of a set.

3.1 Circular Masks

In [5], the masks are designed to have a circular shape in the UV plane. They are expressed by

$$M_L(u,v) = \begin{cases} \min(\hat{E}(u,v)) & \text{for} \quad \mathscr{E}_L(u,v;\Theta_{hp}) > 0 \\ -3 & \text{for} \quad \mathscr{E}_L(u,v;\Theta_{hp}) \le 0 \end{cases}, \tag{8}$$

and

$$M_U(u,v) = \begin{cases} \tau & \text{for} \quad \mathscr{E}_U(u,v;\Theta_{fn}) > 0 \\ 0 & \text{for} \quad \mathscr{E}_U(u,v;\Theta_{fn}) \le 0 \end{cases}, \tag{9}$$

where

$$\mathscr{E}(u,v;\Theta) = (u-u_0)^2 + (v-v_0)^2 - \sin^2(\Theta), \tag{10}$$

Θ_{hp} and Θ_{fn} are the preset HPBW and first-null beamwidth (FNBW) of the main beam, respectively, and τ is the target SLL. The angular coordinates of the main beam in a given direction are represented by (u_0, v_0), which are used to determine the location of the center of the circular mask. It should be noted that 1-bit quantization coding is used in this paper, i.e. Φ_{mn} is selected from only two values, 0 and π.

3.2 Elliptical masks

The resulting beam from the circular mask will not, however, be symmetric in θ and φ, for $\theta_r \neq 0$. As the value of θ_r increases, the HPBW obtained from an elevation slice of the beam will be larger than that from an azimuthal slice. This difference is insignificant when the steering angle is small, but it becomes more obvious as the steering angle increases. To overcome this problem, we substitute the original circular mask with an elliptical projection of the main beam in the UV-plane. The mask is defined as the projection of a circle in the 3D plane. The axis direction is formed by the intersection of a rectangular cone with the center vertex of the surface, the tensor angle Θ_{hp}, and the beam direction as its point of intersection. In other words, the center of the elliptical mask will overlap with that of the circular mask, and the radius r of the long axis of the ellipse will be the same as the radius of the circle. However, the short axis radius in the theta direction (the direction between the center of the ellipse and the center of the RIS) will be $r\cos(\theta_r)$. The expressions of the elliptical masks are given by

$$M_L(u,v) = \begin{cases} \min(\hat{E}(u,v)) & \text{for} \quad \mathscr{E}_L(u,v;\Theta_{hp}) > 1 \\ -3 & \text{for} \quad \mathscr{E}_L(u,v;\Theta_{hp}) \leq 1 \end{cases}, \tag{11}$$

and

$$M_U(u,v) = \begin{cases} \tau & \text{for} \quad \mathscr{E}_U(u,v;\Theta_{fn}) > 1 \\ 0 & \text{for} \quad \mathscr{E}_U(u,v;\Theta_{fn}) \leq 1 \end{cases}, \tag{12}$$

where

$$\begin{aligned} \mathscr{E}(u,v;\Theta) = & \frac{((u-u_0)\cos\alpha + (v-v_0)\sin\alpha)^2}{\sin^2\frac{\Theta}{2}} \\ & + \frac{((u-u_0)\sin\alpha - (v-v_0)\cos\alpha)^2}{\sin^2\frac{\Theta}{2}\cos^2\theta_r}, \end{aligned} \tag{13}$$

and

$$\alpha = \varphi_r + \frac{\pi}{2}, \tag{14}$$

(θ_r, φ_r) are the spherical coordinates of the main beam.

4 Simulation Results

In this section, we show some simulation results for circular and elliptical masks, respectively, by using the optimization approach described in the previous section. For the simulations optimized with GA in this paper, we use the Unified Non-dominated Sorting Genetic Algorithm III (U-NSGA-III) algorithm in pymoo [11], with a configured population size of $W = 1000$, Binomial Crossover with $P_c = 0.9$, Gaussian Crossover with $P_m = 0.1$ and Latin Hypercube Sampling, for $G = 400$ generations. Figure 2 (a) and (b) shows the phase matrices obtained using the GA-optimized circular and elliptical masks for the target HPBW, $\Theta^t = 20^\circ$, $\tau = -18$, $\theta_r = 40^\circ$, and $\varphi_r = 0^\circ$. Then, Figures 2 (c) and (d) show the far-field radiation patterns obtained from the two matrices in Figure 2, respectively. Tables 1 and 2 present the resulting beam widths and SLLs with the circular and elliptical masks for different steering angles, respectively.

Tables 1 and 2 demonstrate that for the same target HPBW Θ^t, as the steering angle θ_r increases, the SLL generated by the circular mask increases, as well as the directivity D decreases; while in the case of the same θ_r, they also show the same trend with increasing Θ^t, as we expected. This can also be observed in the elliptical mask cases as well. Furthermore, it is worth noting that the elliptical mask outperforms the circular mask in terms of both SLL and directivity at larger steering angles.

Additionally, as the steering angle increases, the circular mask generates a main beam with a larger θ dimension, whereas the elliptical mask produces a more uniform main beam with dimensions closer to each other in both θ and ϕ directions. Moreover, using the circular mask, we are unable to generate a beam with $\Theta^t = 20^\circ$ at $\theta_r = 60^\circ$, unlike with the elliptical masks.

As stated in Section 3.2, when the steering angle increases, the circular mask generates a main beam with a larger θ dimension than the ϕ dimension, which becomes increasingly apparent. The UV-plane radiation patterns in Figure 2 (c) and (d) show that with $\theta_r = 40^\circ$ and $\varphi_r = 0^\circ$, the difference between the two results in a more homogeneous main beam. Tables 1 and 2 also indicate that the θ dimension in Figure 2 (d) is smaller than that in Figure 2 (c). During GA optimization, the elliptical masks are larger in the region where SLL needs to be controlled and smaller in the region where HPBW needs to be ensured, compared to the circular masks. That better balances the weights between the two metrics, resulting in a better performance.

5 Conclusion

This paper presents an optimization method based on a genetic algorithm that can generate wide beams while controlling the SLL using two different mask shapes. Simulation results indicate that the beams obtained from the elliptical masks, especially the larger beams, are more uniform in width than those generated by the circular masks, particularly off-broadside. As a first future direction of the work, we will extend our system model to a multi-user scenario involving multiple Tx feeders. Another direction, for our future studies, will be the use of deep learning for beam shaping and widening.

6 Acknowledgements

This work has been done in context of the MESANGES Project ANR-20-CE25-0016-01.

References

[1] W. Tang, M. Chen, X. Chen, J. Dai, Y. Han, M. Renzoet al., "Wireless communications with reconfigurable intelligent surface: path loss modeling and experimental measurement", *IEEE Transactions on Wireless Communications*, **20**, 1, pp. 421–439, Jan. 2021, doi: 10.1109/TWC.2020.3024887.

[2] C. Fonteneau, M. Crussière, and B. Jahan, "A beam broadening method for phased arrays in wireless communications,"

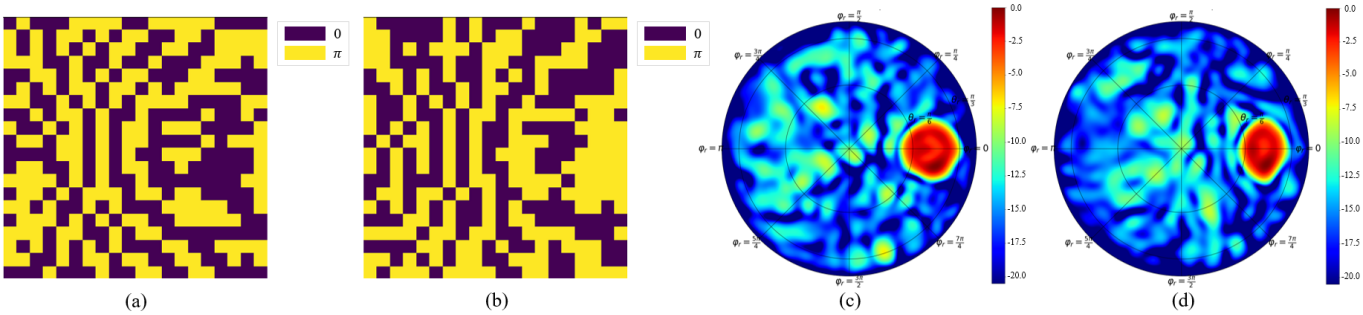

Figure 2. Phase Matrices and Normalized Radiation Patterns obtained using the GA optimized from (a) & (c) the circular and from (b) & (d) the elliptical masks for $\Theta^t = 20°$, $\tau = -18$, $\theta_r = 40°$, and $\varphi_r = 0°$.

Table 1. Beamwidths and SLLs generated for circular masks (Section 3.1) for different steering angles.

θ_r	$\Theta t = 10°$				$\Theta t = 20°$			
	τ (dB)	$\Theta(°):(\theta,\phi)$	SLL (dB)	D(dBi)	τ (dB)	$\Theta(°):(\theta,\phi)$	SLL (dB)	D(dBi)
0°	-25	(10.03, 9.87)	-15.89	23.87	-20	(19.80, 21.20)	-8.52	19.07
20°	-25	(10.73, 10.15)	-13.29	23.23	-20	(22.41, 20.39)	-8.01	18.26
40°	-25	(12.90, 10.15)	-12.23	22.21	-18	(26.99, 21.38)	-7.00	16.98
60°	-25	(21.13, 9.98)	-7.29	19.19	-18			

Table 2. Beamwidths and SLLs generated for elliptical masks (Section 3.2) for different steering angles.

θ_r	$\Theta t = 10°$				$\Theta t = 20°$			
	τ (dB)	$\Theta(°):(\theta,\phi)$	SLL (dB)	D(dBi)	τ (dB)	$\Theta(°):(\theta,\phi)$	SLL (dB)	D(dBi)
0°	-25	(10.03, 9.87)	-15.89	23.87	-20	(19.80, 21.20)	-8.52	19.07
20°	-25	(10.10, 10.09)	-14.71	23.52	-20	(19.75, 20.33)	-6.66	18.44
40°	-25	(9.82, 9.86)	-13.88	23.24	-18	(20.28, 22.13)	-8.37	17.64
60°	-25	(13.04, 9.98)	-9.84	20.79	-18	(20.77, 20.44)	-4.37	16.06

Eurasip Journal on Wireless Communications and Networking, **2022**, 91, Sep. 2022, doi: 10.1186/s13638-022-02173-9.

[3] R. F. Mofrad, R. A. Sadeghzadeh and S. Alidoost, "Comparison of antenna beam broadening methods for phased array radar applications," *2011 Loughborough Antennas and Propagation Conference*, Loughborough, UK, 2011, pp. 1-4, doi: 10.1109/LAPC.2011.6114119.

[4] B. Daniel, C. K. Edwards, and A. W. Anderson, "Phase-Only beam broadening of contiguous uniform subarrayed arrays utilizing three metaheuristic global optimization techniques," *arXiv (Cornell University)*, Sep. 2020, doi: 10.48550/arxiv.2009.06123.

[5] M. Al Hajj, K. Tahkoubit, H. Shaiek, V. Guillet and D. L. Ruyet, "On Beam Widening for RIS-Assisted Communications Using Genetic Algorithms," *2023 Joint European Conference on Networks and Communications and 6G Summit (EuCNC/6G Summit)*, Gothenburg, Sweden, 2023, pp. 24-29, doi: 10.1109/EuCNC/6GSummit58263.2023.10188311.

[6] I. Mallioras, Z. D. Zaharis, P. I. Lazaridis, V. Poulkov, N. V. Kantartzis and T. V. Yioultsis, "An Adaptive Beamforming Approach Applied to Planar Antenna Arrays Using Neural Networks," *2022 IEEE International Black Sea Conference on Communications and Networking (BlackSeaCom)*, Sofia, Bulgaria, 2022, pp. 293-297, doi: 10.1109/BlackSeaCom54372.2022.9858302.

[7] A. Clemente, L. Dussopt, R. Sauleau, P. Potier and P. Pouliguen, "Focal Distance Reduction of Transmit-Array Antennas Using Multiple Feeds," *IEEE Antennas and Wireless Propagation Letters*, **11**, pp. 1311-1314, 2012, doi: 10.1109/LAWP.2012.2227105.

[8] P. Nayeri, *Advanced Design Methodologies and Novel Applications of Reflflectarray Antennas*, Ph. D dissertation, University of Mississippi, 2012.

[9] T. Shan, X. Pan, M. Li, S. Xu, and F. Yang, "Coding Programmable Metasurfaces Based on Deep Learning Techniques," *IEEE Journal on Emerging and Selected Topics in Circuits and Systems*, **10**, 1, pp. 114–125, Mar. 2020, doi: 10.1109/JETCAS.2020.2972764.

[10] W. P. M. N. Keizer, "APAS: An Advanced Phased-Array Simulator," *IEEE Antennas and Propagation Magazine*, **52**, 2, pp. 40–56, Apr. 2010, DOI: 10.1109/ MAP.2010.5525565.

[11] J. Blank and K. Deb, "Pymoo: Multi-Objective Optimization in Python," *IEEE Access*, **8**, pp. 89 497–89 509, 2020, doi: 10.1109/ACCESS.2020.2990567.